3D Ultrasound Image Guidance and Therapy through the Rib Cage with a Therapeutic Random Phased Array

Muhammad Zubair
Department of Bioengineering
Imperial College London
London, UK
m.zubair14@imperial.ac.uk

Sevan Harput
Department of Bioengineering
Imperial College London
London, UK
s.harput@imperial.ac.uk

Robert J. Dickinson
Department of Bioengineering
Imperial College London
London, UK
robert.dickinson@imperial.ac.uk

***Abstract*—Therapeutic and imaging capabilities of a 1 MHz random phased array are described. Multiple simultaneous foci were generated and steered in simulations as well as experimentally. In imaging mode, the random phased array was integrated with Verasonics system via custom-built connectors to acquire raw RF data. Synthetic Aperture Imaging technique was combined with 3D beamforming to achieve 3D volumetric images of the region of interest. In vitro and ex vivo ribs models were imaged both in simulation and experimentally in water bath.**

***Index Terms*—component, formatting, style, styling, insert**

I. Introduction

Focused ultrasound has been used or proposed for many non-invasive surgeries and is capable of treating wide variety of ailments and disorders. A major hindrance in its wide clinical use is the lack of reliable and real time imaging modality and its reliance on MR guidance, which is expensive and is not real time. On the other hand, Ultrasound guidance High Intensity Focused Ultrasound (HIFU) suffers from low resolution, limited field of view and limited penetration depth. Imaging with therapeutic array has emerged as an alternative technique to guide and monitor the HIFU treatment, in which single transducer is used for both imaging and therapy and thus does not suffer from alignment problems. However, therapeutic arrays are concave or spherical in shape with low f-number and has large, directive elements randomly positioned on a shell, so they are not ideal for imaging. This necessitate the use of synthetic aperture imaging (1; 2) and signal processing of echo data to improve spatial resolution. Use of phased arrays for both therapy and imaging has been investigated by Ebbini in (3; 4).

Imaging with the therapeutic array can be a useful tool to overcome a major problem in clinical HIFU, the ablation of tissue underlying the ribs. Sufficient energy should be transmitted through the ribs to induce tissue necrosis without overheating the ribcage as it will lead to skin burns. Several techniques have been proposed to overcome this problem and determine the efficacy of transcostal HIFU. Wu et. al. resected a portion of the ribs shadowing the targeted region in order to provide acoustic window (5). The use of phased array to sonicate the liver tumour between the ribs was suggested in late 1990s but could not be tested experimentally (6; 7; 8) . Civale et. al. used a linearly segmented transducer to lower the temperature on the ribs but the remaining elements were not able to produce sufficient energy(9). Liu 2007 deactivated array elements being obstructed by the ribs to minimize heat deposition over the ribs in a numerical study (10). Cochard et. al. used a method based on DORT by analysing backscattered echoes from ex-vivo ribs immersed in water and deactivated the blocked elements in order to minimize heat on the ribs (11). Quesson et. al. described a method to enable intercostal HIFU ablation while sparing ribs and surrounding tissues (12). The method selected elements based on the relative location of focal point and anatomical images of ribs prior to heating. The technique was implemented both ex-vivo and in-vivo but it relies on MRI images to identify the rib cage and turn off the blocked elements. Aubry et al. used time reversal technique to focus through the rib cage and reported a mean temperature increase of only 0.3, however, this technique required an invasive procedure to insert an acoustic source at the focal point. Bobkova et al. quantified the parameters of focus splitting and determined that the rib cage acts as an aberrator (13).

In this work, we show that random phased array is capable of detecting and imaging obstruction that lie in the therapeutic beam path. We have further shown that sets of multiple foci can be generated and steered in the treatment volume in different regions without any bones obstruction such as uterine fibroid and with bone hindrance such as liver. The suitability of random phased array for imaging the rib cage in simulation and experiments is demonstrated.

Identify applicable funding agency here. If none, delete this.

II. MATERIALS AND METHODS

A. Acoustic Field Modeling

Pressure for each plane circular element was calculated analytically using the expression (14):

$$P_i(\theta, r) = \frac{ip_0 Z_R e^{ikr}}{r} \frac{2J_1(kasin\theta)}{kasin\theta} \tag{1}$$

where p_0 is the pressure on elements surface, a a is radius of the element, k is the wave number, $Z_R = \frac{ka^2}{2}$ is the Rayleigh length, r is the distance from the element center to the field point and J_1 is the first order Bessel function. Total field of the array is obtained by summing field contributions from all the elements

$$P(r) = \sum_i P_i(\theta, r) \tag{2}$$

For a particular focus configuration, the distribution of phases and velocity for each element is calculated using the pseudoinverse method mentioned (15) and described by Ebbini and Cain 1991 as follows:

$$u = H^{*t}(HH^{*t})^{-1}p \tag{3}$$

The intensity distribution was calculated both in the ribs plane and in the focal plane from the pressure distribution as

$$I(x, y, z) = p^2/2\rho c \tag{4}$$

Where p is the pressure amplitude.

B. The Array Transducer and RF control system

The array transducer is similar to the one described in (15) and consisted of 256-elements each 7 mm in diameter, with a minimum inter-element spacing of 7.9 mm and maximum spacing of 9.4 mm. The elements are distributed randomly on a spherical surface with a radius of curvature of 130 mm and diameter of 170 mm. There is a centre aperture hole of 38 mm in diameter in the centre of the array to accommodate a separate imaging transducer, which is not utilized in this work. The array is excited with a burst pulse with frequency of 1 MHz. The operational frequency range is 0.8 to 1.2 MHz. The maximum acoustic power that could be delivered by each element is approximately 2.3 W. A commercially available driving system was used to generate and control RF signals given to the system at 1 MHz operating frequency. Four RF outputs provided power to the four quadrants of the array. The generator was controlled by laptop computer and relative phased were provided through a text file to select active channels.

C. Synthetic Transmit Aperture Imaging

Multiple synthetic aperture beamforming techniques were used to assess the imaging capabilities of the random phased array. Among them, synthetic transmit aperture (STA) performed the best. In STA, one element acts as transmitter and all elements receive the echo. The system is in focus at every voxel of the 3D image thus providing full dynamic focusing in both transmit and receive. Focusing is done by calculating distance between imaging point and transmitting and receiving elements. The image pixel at (x_p, y_p, z_p) is computed using:

$$I(x_p, y_p, z_p) = \sum_{i=1}^{N}\sum_{j=1}^{N} y_{i,j}(\frac{2r}{c} - \tau_{i,j}) \tag{5}$$

Where $y_{i,j}$ is the echo element received by element j when transmitting with element i.

The random phased array was integrated with Verasonics system via custom-built connectors to acquire RF data. Synthetic Aperture 3D beamforming technique was used to achieve 3D volumetric images of the region of interest. Wire phantom was imaged in simulation and metallic rib phantoms and ex-vivo ovine ribs were imaged both in simulation and experimentally in water bath.

III. RESULTS AND DISCUSSION

A. Imaging Results

A wire target array was imaged using the STA approach to determine the spatial resolution as well as the maximum extent of the imaging field of view. Wire targets were placed from -10mm to 10mm in lateral and 100 mm to 130 mm along axial direction. The spacing between each pair of wire is 5mm in lateral and 10mm axially.

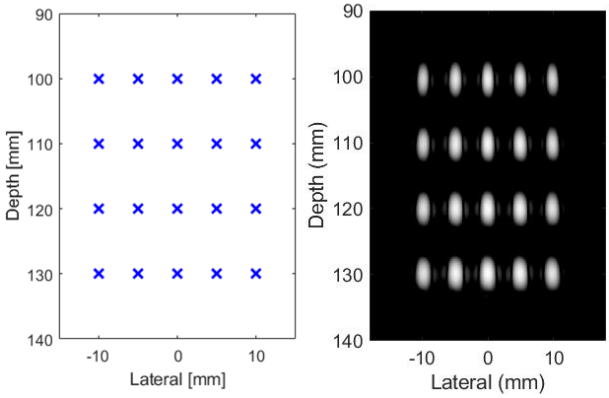

Fig. 1. Simulated Bmode image (30 dB) of a wire phantom

A metallic ball phantom consisting of 3 metallic balls each of radius 8 mm and spacing of 7mm were immersed in water bath and imaged using STA beamforming.

The lateral resolution was determined for STA beamforming for 1 emission and 256 emissions as shown below. The sidelobe level is significantly reduced from -15dB down to -30 dB, whereas the main lobe is also narrowed.

To study the capability of the RPA to image the ribs, two experiments were conducted in which two ovine ribs were placed near the geometric focus in degassed water and a 3D image was obtained.

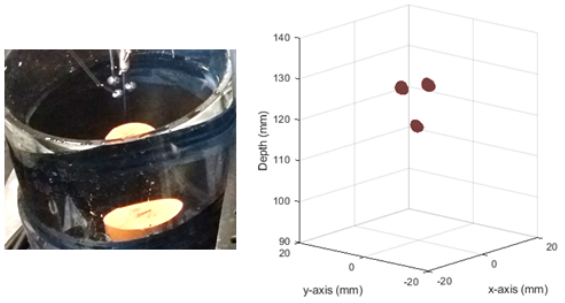

Fig. 2. Experimental setup of two metallic balls with diameter 7mm positioned at $\pm$ 8 mm from geometric focus laterally and one ball is placed at 10mm axially from the focus (left). 3D image (right)

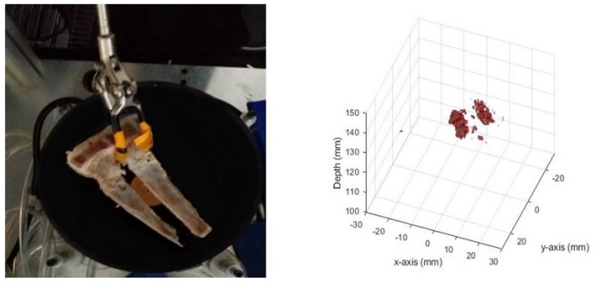

Fig. 3. Experimental setup showing two ovine ribs in degassed water (left). 3D image (right)

B. Ultrasound Intensity distribution in absence of Ribs

Theoretical evaluation of the field distribution was performed at a low acoustic power of 15 W which produced an average intensity of $0.152W/cm^2$ at each of the 256 elements. A single focus targeted at the centre of the curvature of the array has 1.2 mm -6dB full width. The maximum intensity predicted in the focal plane was $388W/cm^2$. Maximum intensity is reduced to $200W/cm^2$ when the focus is steered 15mm off the axis but no secondary hotspots are observed. The focus can thus be steered 3cm laterally and 6 cm along the axis without having significant grating lobes. Sets of five simultaneous foci were generated in circles of 5cm, 8cm and 16 cm in the plane at z = 130mm. It was observed that the maximum intensity for the given acoustic power is $90.5W/cm^2$, $82.5W/cm^2$ and $67.75W/cm^2$ when the spacing between the focus points is $2.5, 4$ and 8 cm, respectively. Sets of five simultaneous foci were also steered in the focal plane and the secondary intensity maxima were below 20% of the peak value. It was possible to steer the pattern of foci upto 15mm off axis at distance between 90mm to 140mm with acceptable level of secondary lobes.

C. Ultrasound Intensity distribution in presence of Ribs

Simulations were performed to demonstrate the effect of ribs on ultrasound focusing and calculate intensity distribution in the rib and focus planes in an xy coordinate grid with spatial step of 0.2 mm. Two rib phantoms were used in simulation. In the first configuration, five parallel strips with a width of 16mm and spacing 18 mm was simulated in MATLAB. The thickness of each strip was 4 mm. The ribcage model was positioned at various heights from the center of the array and geometric ray tracing was performed to determine the elements being blocked by the strips while focusing at the geometric focus of the array. The elements whose normal was crossing any of these strips was deactivated and acoustic field was calculated with the remaining elements. For multiple simultaneous foci, the normals from all elements to each focus was used to find the blocked elements. Intensity distribution in both rib plane and focal planes were calculated. It was observed that the ribs are clearly spared and the energy is distributed only intercostally.

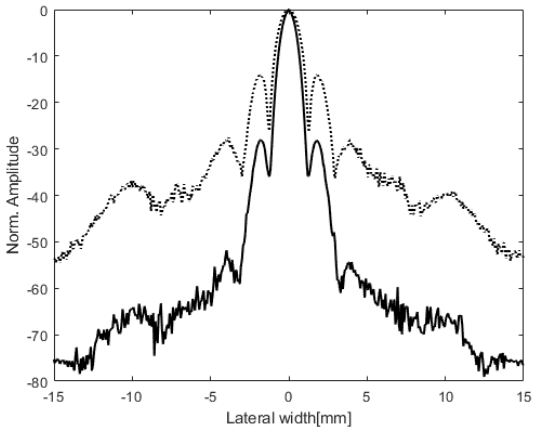

Fig. 4. Lateral beamprofile for STA imaging. The dotted line is for 1 emission and the solid line is for 256 emissions

When the ribs were placed at 40 mm from the array center, only 100 elements were activated and the peak intensity was reduced to 194.2 W/cm^2. When the rib phantom was positioned at a depth of 100mm from the transducer, the number of active elements was changed to 132 and the peak intensity at the focus plane was slightly increased to 198.8 W/cm^2. The focus splitting phenomena was observed. Two secondary lobes at ± 4.5mm were observed off the main lobe with amplitude of 38% of the main lobe. when the rib phantom was positioned at 100mm, the secondary lobes appeared closer to the main lobe at a distance of 1.7mm. The level of secondary lobe increased to 62% of the main lobe.

A rib topology was obtained in STL format from an adult male cadaver. Ribs 8 to 12 of the left side rib cage were used in the simulation after truncating from the spine. A MATLAB function was used to voxelize the phantom. The rib cage was positioned in such a way that the lowest point of the ribs was 39 mm away from the array axially and the highest point was at a distance of 96mm. Rib 9 was straight above the geometric focus.

For a single focus at the geometric focus, it was observed that the secondary lobes were very low as compared to the previous geometries. The peak level in the secondary peaks was only 6% of the main lobe and the spacing from the main

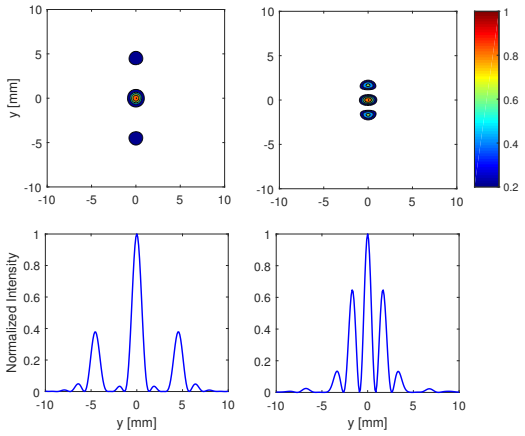

Fig. 5. Position and level of secondary lobes. Top row is the 2-D normalized intensity distribution, bottom row is the corresponding 1-D distribution along y-axis, when the rib phantom is positioned at 40mm depth (left), at 100mm depth(right)

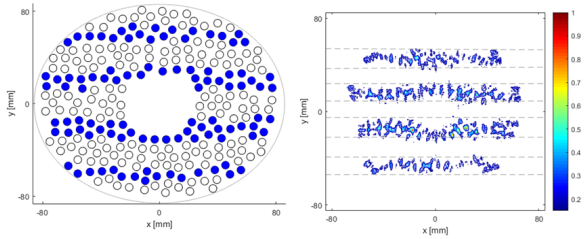

Fig. 6. Distribution of active elements of the array. Filled circles denoted active elements (left). Predicted intensity distribution for a single focus generated at the centre of curvature of the array (0,0,130) mm when the rib phantom was placed at 40mm depth from the array (right). The number of active elements is 100

lobe was 5mm. The reason for the low level of the secondary lobes in rib cage compared to the previous geometry is the varying geometry of the ribs. The ribs in human ribcage are not as periodic as in the simulated geometries shown previously. Moreover, human ribs do not lie in a single plane but are more curved and hence spare the ultrasonic energy to be transmitted intercostally.

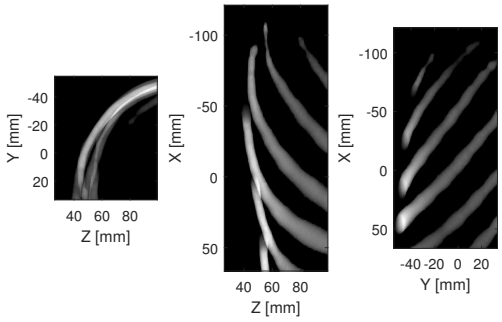

Fig. 7. Ribs 8 to 12 of human cadaver

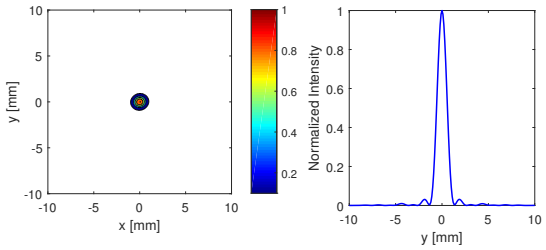

Fig. 8. Intensity distribution in the focal plane when a single focus is generated at (x,y,z) = (0,0,130)mm. Normalized 2D predicted distribution (left), and corresponding 1-D distribution along y-axis

IV. Conclusion

Simulation studies and laboratory tests have shown that random phased array is not only capable of generating and steering single and multiple foci along lateral width and axial depth to ablate the tissue but is also capable of imaging the bone such as ribs. Since integration of an external imaging modality with HIFU is a hindrance in its clinical use, we have shown that such an array is capable of targeting and ablating through the rib cage without overheating the ribs.

References

[1] J. A. Jensen, S. I. Nikolov, K. A. Gammelmark, M. H. Peddersen, "Synthetic aperture ultrasound imaging." Ultrasonics, vol. 44, pp. e5–e15, 2006

[2] I. Trots, A. Nowicki, M. Lewandowski, "Synthetic transmit aperture method in medical ultrasonic imaging",World Academy of Science, Engineering and Technology, vol. 4, pp. 217 – 220, 2010.

[3] E.S. Ebbini, Y. Hui, A. Shrestha. "Dual-mode ultrasound phased arrays for image-guided surgery." Ultrasonic Imaging, vol. 28, no. 2, pp 65 – 82, 2006

[4] A. Haritonova, L. Dalong, E. S. Ebbini "In Vivo application and localization of transcranial focused ultrasound using dual-mode ultrasound arrays." IEEE transactions on ultrasonics, ferroelectrics, and frequency control, vol. 62, no. 12, pp. 2031 – 2042, 2015.

[5] F. Wu, et al. "Extracorporeal high intensity focused ultrasound ablation in the treatment of patients with large hepatocellular carcinoma." Annals of surgical oncology, vol. 11, no. 12, pp. 1061, 2004.

[6] Y. Y. Botros et al. "A hybrid computational model for ultrasound phased-array heating in presence of strongly scattering obstacles." IEEE Transactions on Biomedical Engineering, vol. 44, no. 11, pp. 1039-1050, 1997

[7] Y. Y. Botros, E. S. Ebbini, and J. L. Volakis. "Two-step hybrid virtual array ray(VAR) technique for focusing through the rib cage." IEEE transactions on ultrasonics,

ferroelectrics, and frequency control, vol. 45, no. 4, pp. 989-1000, 1998.

[8] R. J. McGough, et al. ”Treatment planning for hyperthermia with ultrasound phased arrays.” IEEE transactions on ultrasonics, ferroelectrics, and frequency control, vol. 43, no.6, pp. 1074-1084, 1996

[9] J. Civale et al. ”The use of a segmented transducer for rib sparing in HIFU treatments.” Ultrasound in medicine biology, vol. 32, no.11, pp. 1753-1761, 2006.

[10] L. H. Liu et al., ”Feasibility of transrib focused ultrasound thermal ablation for liver tumors using a spherically curved 2D array: A numerical study.” Medical physics, vol. 34, no. 9, pp. 3436-3448, 2007.

[11] E. Cochard et al., ”Ultrasonic focusing through the ribs using the DORT method.” Medical physics, vol. 36, no.8, pp. 3495-3503, 2009

[12] B. Quesson, et al., ”A method for MRI guidance of intercostal high intensity focused ultrasound ablation in the liver.” Medical physics, vol. 37, no. 6, Part1, pp. 2533-2540, 2010.

[13] S. Bobkova et al. ”Focusing of high-intensity ultrasound through the rib cage using a therapeutic random phased array.” Ultrasound in medicine biology, vol. 36, no. 6, pp. 888-906, 2010

[14] H. O’Neil, ”Theory of focusing radiators.” The Journal of the Acoustical Society of America, vol. 21, no. 5, pp. 516-526, 1949

[15] J. W. Hand, et al. ”A random phased array device for delivery of high intensity focused ultrasound.” Physics in Medicine Biology vol. 54, no. 19, pp. 5675, 2009.

[16] E. S. Ebbini, and C. A. Cain, ”A spherical-section ultrasound phased array applicator for deep localized hyperthermia.” IEEE Transactions on Biomedical Engineering, vol. 38, no. 7, pp. 634-643, 1991